Na'ol Kebede and Nabeel Rehemtulla

ASTRO 461

Star Formation Rate in Merger Galaxies

Abstract

One of the main ways to understand galaxy evolution is by looking at the well defined Kennicutt-Schmidt law that describes the relationship between star formation rate density, the mass of new stars per year per area, and gas surface density, which is a measure of the total gas mass per visible surface area. This law has been fit to spiral, (ultra)luminous IR, BzK and elliptical galaxies and shows the same power law relation for all of them. We want to see how galaxy mergers of different types fit into this relation based on their star formation rate density and gas surface density. We look at the Hα band to find their star formation rate densities and collect previously observed data giving us their gas surface density. With these two parameters, we can see how various merger galaxies stand in relation to non-mergers with respect to the Kennicutt-Schmidt law. With a larger sample size, this would give us insight into how the merger galaxies evolve over time and expand our knowledge on star formation in these galaxies of different types.

Background and Methods

When characterizing galaxies, star formation rate is a key component in understanding their evolution. From this we can derive information of the galaxy and understand how different types of galaxies evolve. How galaxies evolve when part of a merger is less well understood, so information on how their star formation rates change

is especially valuable. The Kennicutt-Schmidt law gives us a relationship between the star formation rate density and the gas surface density as

$$log \sum_{SFR} [M_{\odot} yr^{-1} kpc^{-2}] = 1.42 \times log \sum_{gas} [M_{\odot} pc^{-2}] - 3.83 \quad (1)$$

(Daddi, E. et al. 2010)

The power law relationship between these quantities accurately describes the behavior of the different galaxy types. There have been surveys of galaxy categories that include spiral galaxies, BzK galaxies, Luminous IR galaxies, and quasi stellar objects. However, there has been no data taken on galaxy mergers. Galaxy mergers are interesting in that we don't have much data on how the dynamics of the interactions between the galaxies affect the behavior we are accustomed to with non-merging galaxies. When the collisions of objects are on this scale, it is be difficult to see how they change over time.

In order to understand more about the evolution and morphology of galaxies, we investigate how well the galaxy mergers follow this law. We measure the star formation rate through H-alpha imaging and gather gas surface density from cataloged gas mass data for mergers in early, mid, and late stages. We also look at different types of mergers like NGC 6786A and 6786B which consists of a larger galaxy absorbing a smaller one. We hope to expand the understanding of how galaxy mergers differ from non-merger galaxies and how they fit into our model for galaxy star formation rate behavior.

In order to compare star formation rates (SFRs) of our merger galaxies to the that of non-mergers we will overlay our merger galaxy data onto a plot of SFR density

versus gas surface density (GSD) with many types of non-merger galaxies. SFR density is simply the SFR divided by the surface area of the disk of the galaxy which helps normalize the metric. Because we cannot directly measure SFR or GSD we need to introduce measurable quantities that relate to and can be used to calculate SFR and GSD. In the past, this has been done for SFR with a simple conversion from luminosity of Hα emission to SFR. Hα acts as an indicator for star formation because newly formed stars are predominantly located near molecular clouds. The light from these young stars interacts with the gas in the clouds, ionizing the hydrogen atom. After this, the electron and proton recombine to make a new hydrogen atom. The electron may be in any energy level and will drop to the ground state, emitting a photon. About half of the time, the electron will go from the n=3 to n=2 state, which will emit an Hα photon.

$$SFR(M_{\odot}yr^{-1}) = \frac{L(H\alpha)}{1.26\times10^{41} ergs\, s^{-1}} \quad (2)$$

(Kennicutt, R. et al. 1998)

The analogous solution to calculating GSD with a measurable quantity is observing CO luminosity. The underworkings of this conversion are more complicated, but it is essentially done by inferring the mass of molecular Hydrogen in the galaxy, which makes up almost all of the gas mass, based on typical mass percent compositions in galaxies and the amount of CO we know to be there from its measured luminosity. This gives us a good idea of the total gas mass in the galaxy. From this we can calculate the GSD by dividing the gas mass by the visible surface area of the galaxy.

The 1.3m McGraw Hill telescope is capable of observing the Hα band we need in order to calculate SFR for our target galaxies, but neither of the telescopes here at MDM can observe the relevant CO lines as they exist in the radio wavelength regime. Thus, we have selected four target merger galaxies for which the necessary CO or gas mass data exists and we will observe Hα to calculate SFR. With these two components we can connect back to the accepted relation between SFR and GSD to see how these merger galaxies compare to non-merger galaxies. Three of our four galaxies are at a redshift of $z \geq 0.02$, which causes the Hα line to be redshifted enough such that it will not lie within the transmission range of the standard Hα filter. To remedy this, we are using the redshift Hα filter at a shift of +13nm which now captures the Hα lines of our more distant redshifted galaxies. We also need a second Hα filter to do continuum subtraction to verify the Hα we receive is from star formation and not from starlight.

Observing

We took exposures of four galaxy merger cases: NGC 4567, NGC 4676, NGC 6786 and NGC 6240. They were chosen because of our limitations in time and telescope capability and also because they each stood at a different stage in their mergers. NGC 4567 is starting to merge, NGC 4676 is in the process of merging, NGC 6240 recently coalesced and NGC 6786 is a system with a larger galaxy absorbing a smaller one. These systems fit with our limits because they all lied at air masses near 1, were bright enough to get enough signal to noise with a relatively short exposure (less than an hour) and most importantly because we could find previously measured gas mass data for them which we used in calculating their GSDs.

We observed on May 10th, May 12th and May 13th. On the 10th, we took a 600 second exposure of NGC 4567, a 1200 second exposure NGC 4676, and a 900 second exposure of NGC 6240. We also took exposures of the Ring Nebula and NGC 6790, both planetary nebula, which we will later use as standards for calibrating the photometry of our science targets.

We were unable to take Hα or Hα+13nm flats on the 10th because of time constraints. On the 12th, we took two 900 second exposures of NGC 6786 and standard images of IC 4593. On the 13th, we took two 900 second exposures of NGC 4676 and two 1200 second exposures of NGC 6786. These two objects were at magnitude 14.7 and 13 respectively, so we had to make sure we integrated for long enough to get adequate signal to noise. We had to rely on two flat field images. One was taken on the 12th for Hα and the other on the 14th for Hα+13nm. There were more flat field images available but they were unusable due to low counts and the readout freezing. Dust rings can be seen on some of the images, however, they do not render the images unusable. The standard we obtained covered air masses from 1 to 1.17 but, our objects spanned from air masses of 1 to 1.3. This was due to a limited pool of observable planetary nebulae and time constraints. We also had issues during the observing run with the guiding on the 1.3 meter causing many of our images to have slightly smeared targets and background stars. This was only a slight issue which didn't affect us much because we only care about the counts we get on the target galaxy. The guiding error also led to larger errors on the size of our galaxies when converting from

pixel size to arcseconds for the GSD because the area of the galaxy became ambiguous.

Data Reduction and Analysis

After the observing run, once we got our data, we started the usual data reduction procedure of creating master biases and flats and subtracting or dividing them out respectively. We wrote code to do this process for us and ran it on the science and calibration images. This process was slightly more involved than usual because all the telescope control computers and the CCD were power-cycled in the middle of the observing run causing the residual voltages on the CCD to be different before and after. We did our best to correct for this by separating our biases by day and only matching images from a given day with biases also from that day.

Because some of our images needed longer exposure times to get enough signal, we split what would have been a 40 minute exposure to two 20 minute exposures. This gives avoids accumulating cosmic rays in our image.

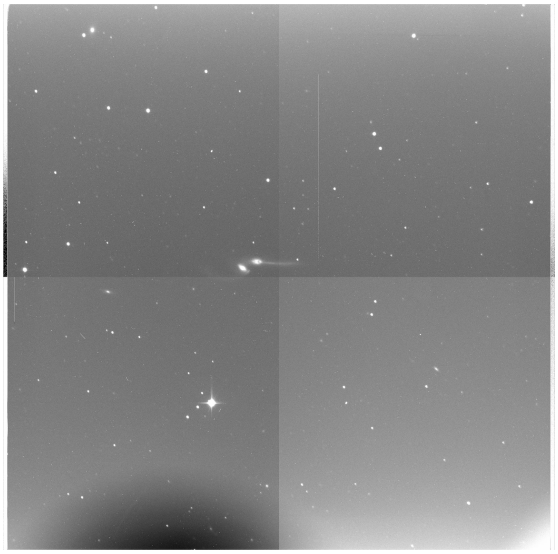

Figure 1: A combination of two exposures of NGC 4676
Hα filter, combination of two 1200 second exposures, 21.3’ field of view, West is up

Figure 1 is an example of combining two 1200 second exposures into a single effectively 2400 second exposure. In order to do science with these targets we need to combine the multiple exposures into a single master exposure after removing bias and flat related noise. This process was not as simple as stacking the images because they were slightly offset, so we picked a few background stars in both images and looked at the difference in their pixel values. With these x and y offsets we wrote code to align and stack the multiple exposures into a single master exposure.

Once we got down to one image in each filter for each target we were ready to start doing continuum subtraction. It is necessary because the light that passes through the Hα filter isn't only from star formation related emission; there is also some starlight at Hα wavelength. In order to get an accurate SFR we need to subtract out the starlight. Again, this wasn't as simple as subtracting one file's pixel values from the other's. First, we needed to align the images in the same way we did for creating the masters: pick background stars, collect pixel offsets, shift image. After we had the images aligned we needed to scale the off-band image such that we subtract the right amount of light. We want to subtract enough such that all the starlight disappears but not subtract too much such that we remove star formation related Hα emission. This is done by collecting flux ratios between the on and off band images. The flux ratios are ratios of counts in the background from the on band over the off band. The counts were collected from a region near the galaxy where only starlight is present to prevent star formation Hα emission being included in the ratio. The off band image counts are divided by this ratio

and then subtracted from the on band. This left us with a single image per target that contained Hα emission from star formation.

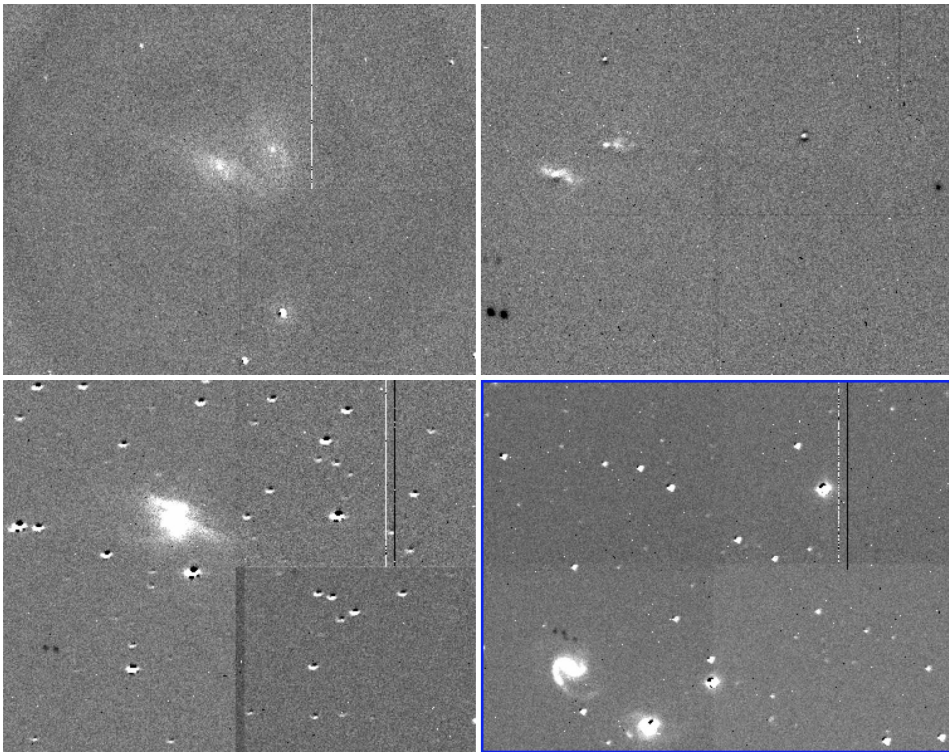

Figure 2: final continuum subtracted images
Top left: NGC 4567, Top right: NGC 4676
Bottom left: NGC 6240, Bottom right: NGC 6786

Figure 5 shows the results of the continuum subtraction. As mentioned earlier, we had issues with the guiding system on the 1.3m McGraw Hill telescope causing background stars in some of our images to be streaked. This prevents the background stars from disappearing in our continuum subtracted images despite the ratio being correct. We know the ratios to be correct because we see negative and positive regions of counts on the background stars with similar absolute values. If the guiding was perfect and counts were distributed identically, the positive and negative regions of counts would overlap and cancel. You can see this effect in Figure 2. For all the targets

except NGC 4567, Hα+13 was the on band and Hα was the off band, so we subtracted the Hα image from the Hα+13 image. The opposite is true for NGC 4567. Figure 3 shows the continuum subtracted image of NGC 6240 and the residual background stars with the negative and positive regions.

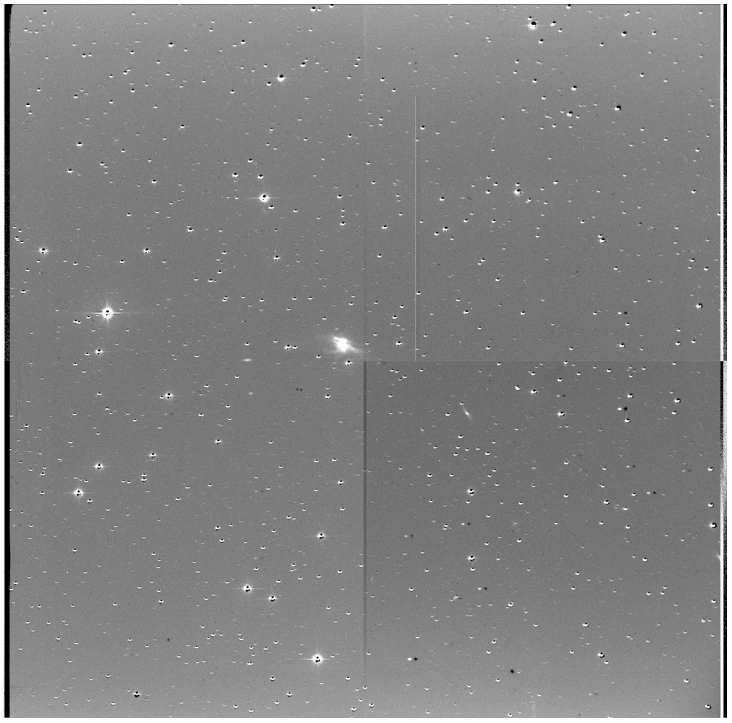

Figure 3: A continuum subtracted image of NGC 6240
Hα+13 - Hα, 21.3' field of view, East is up

The next step was calibrating the astrometry and photometry of our targets. Calibrating the astrometry was as simple as uploading the image to astrometry.net. However, for the images that could not be uploaded, we had to manually . With calibrated astrometry, we had code that would look at the RA and DEC of the object of interest and find the x and y pixel value that it is on. For uncalibrated images, we used DS9 to find the center of the object. These pixel values were used for the centers of the aperture around each source. For our standard images, we used circular apertures.

Because the target galaxies were elongated in shape, we used elliptical apertures. Once the apertures were defined for each of the targets, we use a function called aperature_photometry in photutils to get the flux for the source and a background annulus around each source. We then correct for atmospheric extinction in Hα with equation (3) where c_1 is the Hα extinction coefficient and X is the airmass of the target

$$F_{corr} = F * e^{-0.3 c_1 X} \quad (3)$$

The Hα coefficient was not available on the KPNO website, so we had to infer the value from the R band atmospheric extinction coefficient. After this, the background counts are corrected for and a final flux is determined for the standard. Because the flux of the standard is well known in Hα, we can then use this as a zero point for the science images. The same process is repeated for the science images with aperature_photometry to determine the final flux of the source. We also use the area of the apertures to determine the size of the object in the sky as well as the physical size.

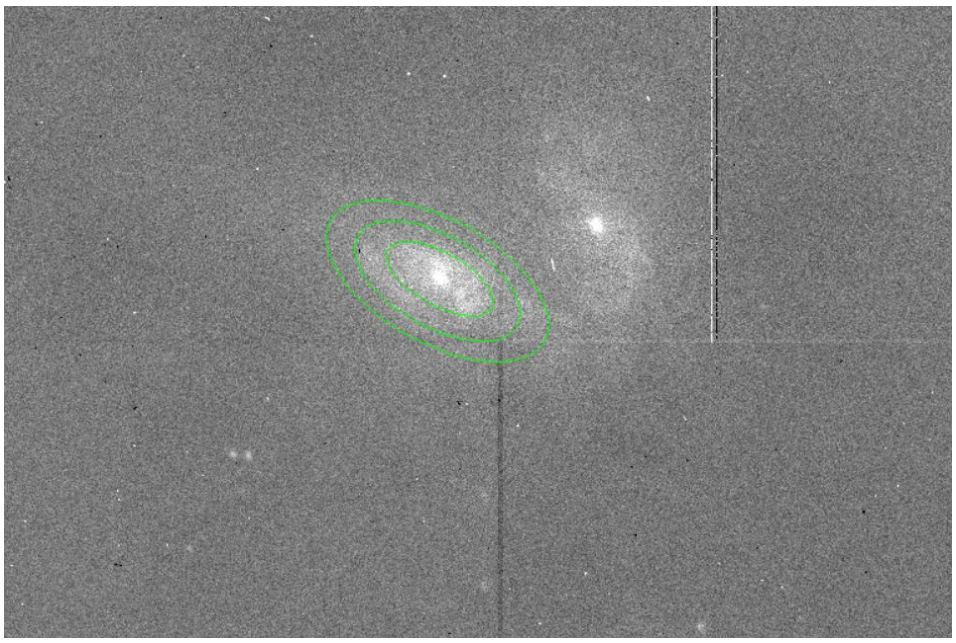

Figure 4: NGC 4567 with elliptical aperture and annulus
Hα - Hα+13, 21.3' field of view, East is up

Figure 4 shows apertures and background annului on NGC 4567 and NGC 4568. For both galaxies, the inner ellipse is the aperture and the outer two ellipses are the inner and outer bounds on the background annulus.

With the photometry completed, we then had flux in units of counts over the drawn aperture's area for each galaxy, and because we calibrated the continuum subtracted images the measured flux was all from star formation. We used the flux of the standards, which are well known, to scale with the counts on the standards and science targets to get flux of the science images. The flux then goes through a chain of conversions. First, it is converted to luminosity with the familiar equation $L(H\alpha) = 4\pi d^2 F$ where we have d as the distance to the galaxy in centimeters and F as the flux in $\frac{ergs}{s\ cm^2}$. The luminosity is then fed into the widely accepted and used equation (2) which . The last step simply has us divide the SFR by the deprojected area, basically the surface area of the disk, as described by Kennicutt et al. 1998. This leaves us with SFR density which we take the log of and plot it versus the log of GSD. With this plot we can compare the SFR as a function of GSD of our merger galaxies with that of the range of galaxies that the Kennicutt-Schmidt law applies to.

Table 1: data on calculated and observed quantities for our four target merger galaxies

Targets	NGC 4567	NGC 4676	NGC 6786	NGC 6240
Exposure times in each band (s)	600	1200, 900, 900	900, 900	900
Galaxy distance	22.45[1]	101.44[2]	109.21[3]	108.67[4]

(Mpc)				
Projected surface area (kpc^2)	637.14	1030.24	1838.66	2083.67
Disk radius (kpc^2)	24.4[2]	107.86[2]	39.81[2]	74.97[2]
H α Flux $\frac{ergs}{s\ cm^2}$	$4.42 * 10^{-12}$	$7.92 * 10^{-13}$	$3.55 * 10^{-12}$	$6.74 * 10^{-13}$
log(GSD) $(M_\odot pc^{-2})$	0.63[5]	1.58[6]	1.08[7]	1.75[8]
log(SFR density) $(M_\odot yr^{-1} kpc^{-2})$	-2.48	-2.12	-1.66	-2.44

[1] de Vaucouleurs et al. 1981, [2] Jarett et al. 2003, [3] Falco et al. 1999, [4] Downes et al. 1993
[5] Kaneko et al. 2013, [6] Yun et al. 2000, [7] Mirabel et al. 1990, [8] Wilson et al. 2008

Table 1 shows the results of our calculations and the numbers we pulled from other sources. The final values are plotted on Figure 4.

Results

Once we ran through the data reduction and analysis procedure on all four of our targets using standards for photometric calibrations we are left with SFR density and GSD for four merger galaxies. We compare our results to equivalent quantities for other types of galaxies by overlaying the data points onto a well populated plot of the Kennicutt-Schmidt law from Daddi et al. 2010.

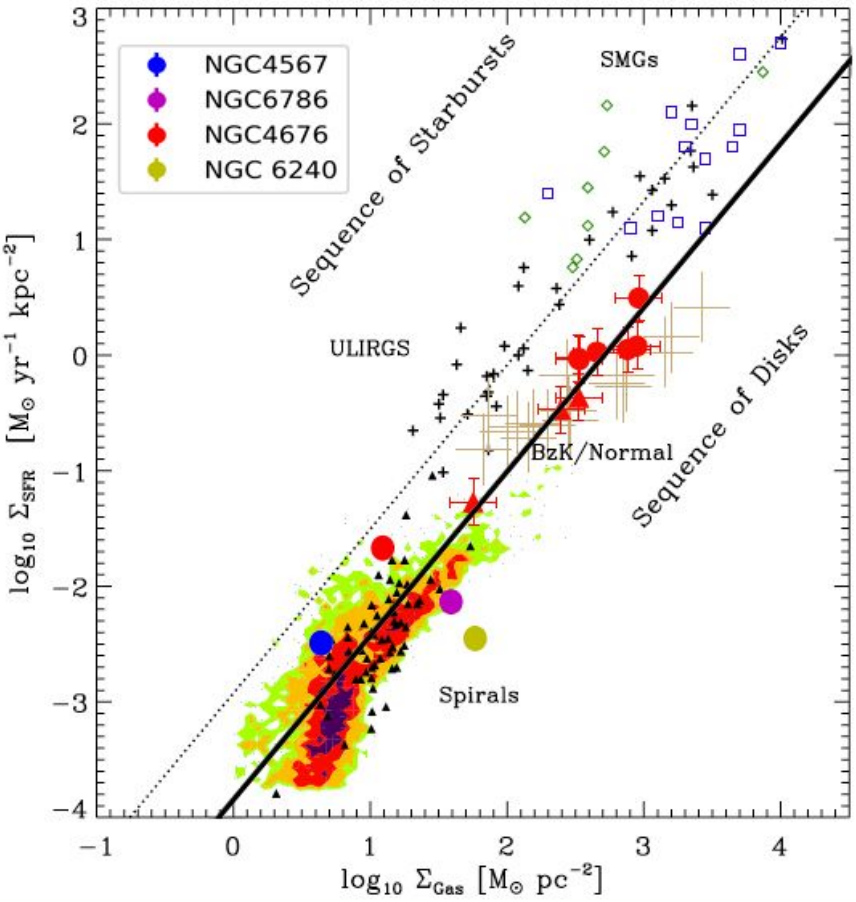

Figure 5: SFR density vs GSD with Kennicutt-Schmidt law, regions for types of galaxies and our results overlayed in black points with error-bars
Original plot from Daddi, E. et al. 2010

Figure 5 shows our four merger galaxies and their SFR in the context of other galaxies. NGC 4567 and NGC 6786 both lie above the standard sequence of disk galaxies and near the sequence of starburst galaxies. NGC 4676 lies in line with spiral galaxies of similar GSD, and NGC 6240 lies below the Kennicutt-Schmidt law curve. The error bars on these points come from the error in the flux of the standards. We generated the error bars by running the error on the flux through our code to see what difference in SFR density they correspond to. Because of the small sample size, it is next to impossible to make broader claims on SFR in merger galaxies. This does, however, act as a robust

proof of concept for the use of small ground based telescopes in investigating SFR of merger galaxies. We were not able to get error bars in the x-axis because we did not have errors on the molecular gas mass collected from various publications.

Conclusion

Star formation rate in galaxies is often outlined by the Kennicutt-Schmidt law which relates star formation rate density to gas surface density with a power law. The Kennicutt-Schmidt law has been applied to many categories of galaxies, however, there is an absence of data on merger galaxies. As an understudied category of galaxies, merger galaxies are hard to quantify in terms of galactic metrics and little is know about their dynamics. With our small sample of data, we were able to show these large scale events do lie on the Kennicutt-Schmidt law, but more Kennicutt-Schmidt law data is needed to define their trend and refine how they are distributed compared to other galaxy categories.

References

Daddi, E., Elbaz, D., Walter, F., Bournaud, F., Salmi, F., Carilli, C., . . . Riechers, D. (2010). Different Star Formation Laws For Disks Versus Starbursts At Low And High Redshifts. *The Astrophysical Journal,714*(1). doi:10.1088/2041-8205/714/1/l118

Downes, D., Solomon, P. M., & Radford, S. J. (1993). Molecular gas mass and far-infrared emission from distant luminous galaxies. *The Astrophysical Journal,414*. doi:10.1086/186984

Falco, E., Kurtz, M., Geller, M., Huchra, J., Peters, J., Berlind, P., . . . Elwell, B. (1999). The Updated Zwicky Catalog (UZC). *Publications of the Astronomical Society of the Pacific,111*(758), 438-452. doi:10.1086/316343

Frew, D. J., Bojičić, I. S., & Parker, Q. A. (2013). A catalogue of integrated Hα fluxes for 1258 Galactic planetary nebulae. *Monthly Notices of the Royal Astronomical Society, 431*(1), 2-26. doi:10.1093/mnras/sts393

Jarrett, T. H., Chester, T., Cutri, R., Schneider, S. E., & Huchra, J. P. (2003). The 2MASS Large Galaxy Atlas. *The Astronomical Journal,125*(2), 525-554. doi:10.1086/345794

Kaneko, H., Kuno, N., Iono, D., Tamura, Y., Tosaki, T., Nakanishi, K., & Sawada, T. (2013). Properties of Molecular Gas in Galaxies in Early and Mid Stages of the Interaction. I. Distribution of Molecular Gas. *Publications of the Astronomical Society of Japan,65*(1), 20. doi:10.1093/pasj/65.1.20

Kenney, J. D. (n.d.). The mass dependence of CO and HI emission in SC galaxies. *Molecular Clouds in the Milky Way and External Galaxies Lecture Notes in Physics,*367-374. doi:10.1007/3-540-50438-9_306

Kennicutt, J. R. (1998). The Global Schmidt Law in Star‐forming Galaxies. *The Astrophysical Journal,498*(2), 541-552. doi:10.1086/305588

Kennicutt, R. C. (1989). The star formation law in galactic disks. *The Astrophysical Journal,344*, 685. doi:10.1086/167834

Mirabel, I. F. (1990). CO(1-0) emission from luminous infrared galaxies in the southern hemisphere. *Astronomy and Astrophysics,236*, 327-332.

Vaucouleurs, G. D., Peters, W. L., Bottinelli, L., Gouguenheim, L., & Paturel, G. (1981). Hubble ratio and solar motion from 300 spirals having distances derived from H I line widths. *The Astrophysical Journal,248*, 408. doi:10.1086/159166

Wilson, C. D., Petitpas, G. R., Iono, D., Baker, A. J., Peck, A. B., Krips, M., . . . Yun, M. S. (2008). Luminous Infrared Galaxies with the Submillimeter Array. I. Survey Overview and the Central Gas to Dust Ratio. *The Astrophysical Journal Supplement Series,178*(2), 189-224. doi:10.1086/590910

Yun, M. S., Verdes-Montenegro, L., Olmo, A. D., & Perea, J. (1997). Molecular Gas and Infrared Emission in HCG 31 and HCG 92 (Stephans Quintet) and Tidal Interactions in Compact Group Environment. *The Astrophysical Journal,475*(1). doi:10.1086/310458

Yun, M. S., & Hibbard, J. E. (2001). Molecular Gas in Optically Selected Mergers. *The Astrophysical Journal,550*(1), 104-121. doi:10.1086/319697